

Thermodynamic properties in the molecular dynamics ensemble applied to the Gaussian core model fluid

Peter Mausbach¹ and Richard J. Sadus^{2,a)}

¹Cologne University of Applied Sciences, 50679 Cologne, Germany

²Centre for Molecular Simulation, Swinburne University of Technology, P.O. Box 218, Hawthorn, Victoria 3122, Australia

(Received 20 December 2010; accepted 8 February 2011; published online 17 March 2011)

The thermodynamic properties of pressure, energy, isothermal pressure coefficient, thermal expansion coefficient, isothermal and adiabatic compressibilities, isobaric and isochoric heat capacities, Joule–Thomson coefficient, and speed of sound are considered in a classical molecular dynamics ensemble. These properties were obtained using the treatment of Lustig [J. Chem. Phys. **100**, 3048 (1994)] and Meier and Kabelac [J. Chem. Phys. **124**, 064104 (2006)], whereby thermodynamic state variables are expressible in terms of phase-space functions determined directly from molecular dynamics simulations. The complete thermodynamic information about an equilibrium system can be obtained from this general formalism. We apply this method to the Gaussian core model fluid because the complex phase behavior of this simple model provides a severe test for this treatment. Waterlike and other anomalies are observed for some of the thermodynamic properties of the Gaussian core model fluid. © 2011 American Institute of Physics. [doi:10.1063/1.3559678]

I. INTRODUCTION

In a classical molecular dynamics (MD) simulation only a few thermodynamic state variables like the pressure and the temperature are calculated. This means that additional methods such as equations of state or fluctuation theory approaches have to be used for the calculation of other thermodynamic properties of the system. However, it was shown by Lustig^{1–4} and recently Meier and Kabelac⁵ that there is a straightforward way to set up the complete thermodynamics via a general statistical mechanical formalism. In principle, this method allows a systematic and rigorous calculation of thermodynamic derivatives to arbitrary order without any restrictive approximations commonly required by conventional approaches such as equations of state. Lustig^{1–4} showed that it is possible to calculate thermodynamic state variables from key derivatives obtained directly from either molecular dynamics or Monte Carlo (MC) simulations.

The method is based on the exact expressions for the thermodynamic state variables reported by Pearson *et al.*⁶ for the microcanonical ensemble or NVE ensemble using a Laplace transform technique. Çağın and Ray⁷ used this technique to derive expressions in the molecular dynamics ensemble or NVEP ensemble. This is a subset of the NVE ensemble where the additional constraint of constant total momentum (\mathbf{P} or equivalently \vec{P}) is used in the formulation of the phase-space volume. Later, Çağın and Ray⁸ applied this approach to a canonical molecular dynamics ensemble or NVTP ensemble and Lustig^{1–4} extended the method to systems of rigid polyatomic molecules. Meier and Kabelac⁵ developed further improvements of this technique for an extended molecular dy-

namics ensemble or NVEPG ensemble with a quantity (\mathbf{G} or equivalently \vec{G}), which is related to the initial position of the center of mass as an additional constant of motion:

$$\vec{G} = \vec{P}t - \sum_{i=1}^N m_i \vec{r}_i(t), \quad (1)$$

where m_i and \vec{r}_i denote the mass and the position of particle i , t is the time and $\vec{P} = \sum_i \vec{p}_i$ is the total momentum of the system.

In this study we apply the extension of Meier and Kabelac⁵ to accurately determine the unusual behavior of the Gaussian core model (GCM) fluid. The bounded GCM potential introduced by Stillinger⁹ has received considerable interest because of its ability to describe properties of soft condensed matter.¹⁰ Furthermore, the GCM fluid displays a rich scenario of waterlike anomalies associated with re-entrant melting behavior.^{11–23} However, the thermodynamic properties of the GCM are far from being completely understood and the occurrence of a whole range of anomalous properties suggest that the GCM possesses unexplored anomalies similar to water, which might have implications for a broad range of waterlike potentials.

The aim of this work is therefore twofold. First, the GCM system provides a severe test for the calculation of thermodynamic state variables using molecular dynamics in the NVEPG ensemble. A successful application of this comprehensive treatment may initiate further studies for systems with unusual thermodynamic properties. Second, we endeavor to complete our understanding of the unusual thermodynamic behavior of the GCM. To the best of our knowledge, the use of the NVEPG ensemble in such a general way has not been reported previously.

^{a)} Author to whom correspondence should be addressed. Electronic mail: rsadus@swin.edu.au.

II. SIMULATION METHOD

A. Brief overview of the method

Lustig¹⁻⁴ showed that in general all thermodynamic state variables could be obtained from derivatives determined directly from MD simulations in a classical NVEP ensemble. In this work, we use the NVEPG ensemble extension of this method developed by Meier and Kabelac⁵ for which entropy $S = S(N, V, E, \vec{P}, \vec{G})$ is the fundamental equation of state for the system. In common with a microcanonical ensemble, this approach involves the number of particles (N), volume (V), and energy (E). However, the total momentum of the system (\vec{P}) and a quantity \vec{G} , which is related to the initial position of the center of mass, are also used as additional constants of motion. Meier and Kabelac⁵ also corrected an error in the general equation for the volume derivatives of the potential energy reported by Lustig.⁴

The fundamental equation of state for the system can be defined by the entropy postulate

$$S(N, V, E, \vec{P}, \vec{G}) = k \ln \Omega(N, V, E, \vec{P}, \vec{G}), \quad (2)$$

where $\Omega(N, V, E, \vec{P}, \vec{G})$ is the phase-space volume and k is the Boltzmann constant. We use Ω instead of the phase-space density ω for reasons discussed elsewhere.⁵ A comparison between the use of Ω and ω is given by Lustig.¹ The basic phase-space functions are then introduced as an abbreviation representing the derivatives of the phase-space volume with respect to the independent thermodynamic state variables E and V :

$$\Omega_{mn} = \frac{1}{\omega} \frac{\partial^{m+n} \Omega}{\partial E^m \partial V^n}. \quad (3)$$

The exact derivation of the phase-space function is quite involved⁵ and is not repeated here. The resulting general expression is given by

$$\begin{aligned} \Omega_{mn} = & V^{-n} (-1)^m \frac{2}{3N-3} \left(-\frac{3N-3}{2} \right)_m (-1)^n (-[N-1])_n \langle K^{-(m-1)} \rangle + (1 + \delta_{0n}) \sum_{i=1}^n \binom{n}{i} (-1)^{n-i} (-[N-1])_{n-i} \\ & \times V^{i-n} \frac{2}{3N-3} \sum_{l=1}^i (-1)^{m+l} \left(-\frac{3N-3}{2} \right)_{m+l} \left\langle K^{-(m+l-1)} \left(\sum_{k=1}^{k \max(i,l)} c_{ilk} W_{ilk} \right) \right\rangle, \end{aligned} \quad (4)$$

and is related to ensemble averages of products of powers of the kinetic energy $K = E - U(\vec{r}^N)$ and of volume derivatives of the potential energy $\partial^n U / \partial V^n$. In Eq. (4), $\langle \dots \rangle$ denotes ensemble averages, $(x)_n = x(x+1)(x+2) \dots (x+n-1)$ represents the Pochhammer symbol with $(x)_0 = 1$ and δ_{ij} is the Kronecker delta. The term $c_{ilk} W_{ilk}$ is a product of certain volume derivatives of the potential energy $W_{ilk} = (-\partial^i U / \partial V^i)(-\partial^k U / \partial V^k) \dots$, and of multinomial coefficients c_{ilk} described in detail elsewhere.⁵ The correct volume derivatives of n th order for the potential energy are given by

$$\frac{\partial^n U}{\partial V^n} = \frac{1}{3^n V^n} \sum_{i=1}^{N-1} \sum_{j=i+1}^N \sum_{k=1}^n a_{nk} r_{ij}^k \frac{\partial^k u}{\partial r_{ij}^k}, \quad (5)$$

where u is the pair potential energy and r_{ij} denotes the distance between particle i and j . The coefficients a_{nk} are constructed using a recursion relation.⁵ All thermodynamic state variables are then expressible in terms of the phase-space function. The derivation of this procedure was described in detail by Lustig¹ and is, therefore, not explained here. The resulting thermodynamic state variables we use in our study are summarized in Table I. Explicit expressions for phase-space functions of low order are given elsewhere.⁵

B. Simulation details

The NVEPG-MD simulations were performed for a homogeneous fluid of 1000 particles interacting via a GCM

potential of the form

$$u(r) = \varepsilon \exp \left[-\left(\frac{r}{\sigma} \right)^2 \right], \quad (6)$$

where ε and σ are the height and width of the potential and r is the distance between two particles. The normal conventions were used for the reduced density ($\rho^* = \rho \sigma^3$), temperature ($T^* = kT/\varepsilon$), energy ($E^* = E/\varepsilon$), pressure ($p^* = p \sigma^3/\varepsilon$), time ($\tau^* = \tau \sqrt{\varepsilon/m\sigma^2}$), heat capacities ($C_{P,V}^* = C_{P,V}/k$), compressibilities ($\beta_{T,S}^* = \beta_{T,S} \varepsilon/\sigma^3$), isothermal pressure coefficient ($\gamma_V^* = \gamma_V \sigma^3/k$), thermal expansion coefficient ($\alpha_p^* = \alpha_p \varepsilon/k$), speed of sound ($w_0^* = w_0 \sqrt{m/\varepsilon}$), and the Joule-Thomson coefficient $\mu_{JT}^* = \mu_{JT} k/\sigma^3$ (m is the mass of the particles). All quantities quoted in this work are in terms of these reduced quantities and the asterisk superscript will be omitted in the rest of the paper.

The simulations covered densities ranging from $\rho = 0.03$ to 1.2 and temperatures ranging from $T = 0.002$ to 3.0 omitting the solid-state region of the model. For low temperatures (up to $T = 0.1$), we used very small temperature increments in order to sample the phase-space region with anomalous phase behavior with high accuracy. The equations of motion were integrated using a five-value Gear predictor-corrector scheme²⁴ with a time step of $\tau = 0.003$. For each state point simulation trajectories were run for 4×10^6 time steps to equilibrate the system. Periods of 12×10^6 time steps were used up to temperatures of $T = 0.3$ and 8×10^6 time steps

TABLE I. Relations of thermodynamic state variables in terms of phase-space functions.

Temperature	$T = \left(\frac{\partial E}{\partial S} \right)_V = \frac{\Omega_{00}}{k}$
Pressure	$p = T \left(\frac{\partial S}{\partial V} \right)_E = \Omega_{01}$
Isochoric heat capacity	$C_V = \left[\left(\frac{\partial^2 S}{\partial E^2} \right)_V \right]^{-1} = k(1 - \Omega_{00}\Omega_{20})^{-1}$
Isothermal pressure coefficient	$\gamma_V = \left(\frac{\partial p}{\partial T} \right)_V = k \frac{\Omega_{11} - \Omega_{01}\Omega_{20}}{1 - \Omega_{00}\Omega_{20}}$
Isothermal compressibility	$\beta_T^{-1} = -V \left(\frac{\partial p}{\partial V} \right)_T = V \left[\frac{\Omega_{01}(2\Omega_{11} - \Omega_{01}\Omega_{20}) - \Omega_{00}\Omega_{11}^2 - \Omega_{02}}{1 - \Omega_{00}\Omega_{20}} \right]$
Isentropic compressibility	$\beta_S^{-1} = -V \left(\frac{\partial p}{\partial V} \right)_S = V[\Omega_{01}(2\Omega_{11} - \Omega_{01}\Omega_{20}) - \Omega_{02}]$
Speed of sound	$w_0^2 = -\frac{V^2}{M} \left(\frac{\partial p}{\partial V} \right)_S = \frac{V^2}{M} [\Omega_{01}(2\Omega_{11} - \Omega_{01}\Omega_{20}) - \Omega_{02}]$
Thermal expansion coefficient	$\alpha_P = \beta_T \gamma_V$
Isobaric heat capacity	$C_P = C_V \frac{\beta_T}{\beta_S}$
Joule–Thomson coefficient	$\mu_{JT} = V \frac{T\gamma_V\beta_T - 1}{C_P}$

for temperatures $T > 0.3$ to accumulate the average values of the thermodynamic state variables. The cut-off radius for the potential was 3.2σ .

III. RESULTS AND DISCUSSION

A. Energy and pressure

The potential energy per particle U/N as a function of temperature at different constant densities is illustrated in Fig. 1. The energy grows monotonically along isochors with increasing temperature and along isotherms with increasing density. Stronger gradients occur at low temperatures and at high densities. In Fig. 2(a), the isochoric temperature depen-

dence of the pressure is shown where the slope of the pressure exhibits a pressure minimum at low temperatures. Figure 2(b) shows a close-up of this region for densities ranging from $\rho = 0.4$ to 1.2. To avoid a large pressure scale the pressure isochors are shifted by values given in Fig. 2(b). The pressure minimum corresponds to the well-known density maximum¹¹ for water at constant pressure. Connecting the points corresponding to the minimum pressure on each isochor defines the so-called temperature of maximum density (TMD) line.¹² Apart from this known anomaly the pressure grows monotonically with increasing temperature and increasing density. The energy and pressure data obtained in this study are in very good agreement with MC simulation results reported elsewhere.^{12,20}

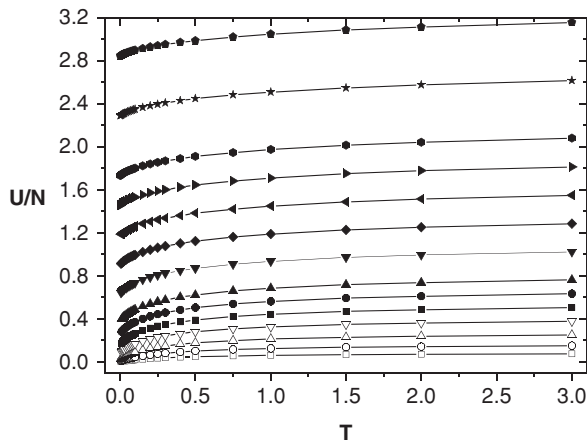


FIG. 1. Potential energy per particle U/N as a function of temperature for different constant densities of $\rho = 0.03$ (\square), 0.06 (\circ), 0.1 (\triangle), 0.15 (∇), 0.2 (\blacksquare), 0.25 (\bullet), 0.3 (\blacktriangle), 0.4 (\blacktriangledown), 0.5 (\blacklozenge), 0.6 (\blacktriangleleft), 0.7 (\blacktriangleright), 0.8 (\bullet), 1.0 (\star), 1.2 (\bullet).

B. Isothermal pressure coefficient

By definition, the isothermal pressure coefficient γ_V becomes negative in phase-space regions with anomalous density behavior. This can be seen clearly in Fig. 3 where the isochoric temperature dependence of γ_V is shown. For densities from $\rho = 0.03$ to 0.2 , γ_V decreases with increasing temperature and develops along the isochor at $\rho = 0.25$, a weak maximum at low temperatures [Fig. 3(b) shows a close-up of this region]. For densities $\rho \geq 0.3$, the temperature dependence of γ_V changes, γ_V increases with increasing temperature. This is an interesting result since $(\partial\gamma_V/\partial T)_V$ changes sign from negative (for $\rho < 0.25$) to positive (for $\rho > 0.25$). The thermodynamic identity

$$T \left(\frac{\partial \gamma_V}{\partial T} \right)_V = T \left(\frac{\partial^2 p}{\partial T^2} \right)_V = \left(\frac{\partial C_V}{\partial V} \right)_T = -\frac{\rho}{V} \left(\frac{\partial C_V}{\partial \rho} \right)_T \quad (7)$$

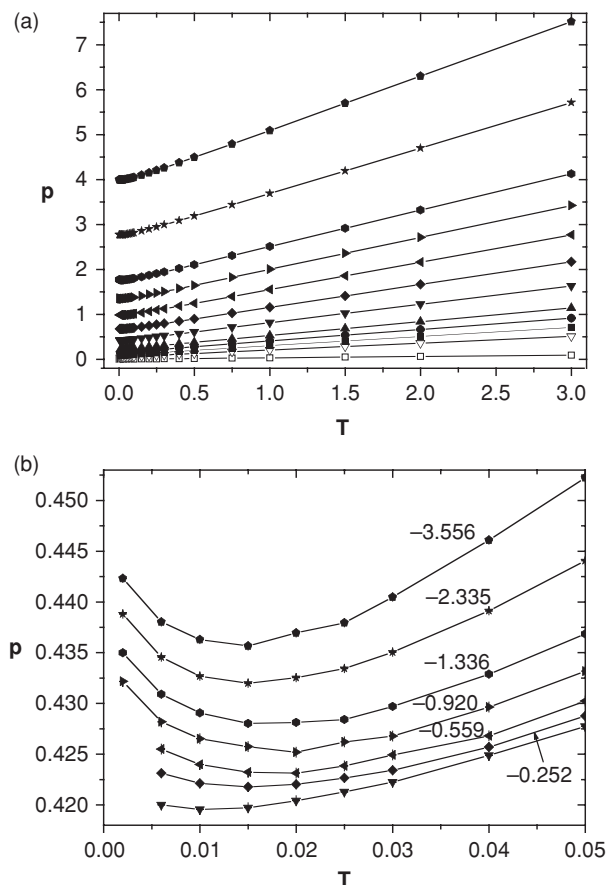


FIG. 2. Pressure as a function of temperature for different constant densities (a) ranging from $\rho = 0.03$ to 1.2 for temperatures up to $T = 3.0$ and (b) ranging from $\rho = 0.4$ to 1.2 for temperatures $T \leq 0.05$. In (b) the pressure isochors are shifted by values indicated on the lines in order to avoid a large pressure scale. Symbols are the same as in Fig. 1.

then implies that the constant volume heat capacity C_V exhibits a maximum along an isotherm in the (ρ, T) plane. For densities $\rho \geq 0.4$, γ_V becomes negative at low temperature where $\gamma_V = 0$ again defines the TMD line.

C. Isothermal and adiabatic compressibilities

In Fig. 4 the isothermal compressibility β_T as a function of temperature at different constant densities is illustrated. The isothermal compressibility decreases sharply with increasing temperature for densities ranging from $\rho = 0.03$ to 0.1 [see Fig. 4(a)] whereas the slopes of β_T for densities $\rho \geq 0.2$ exhibit a maximum at low temperature [see inset of Fig. 4(a)]. In Fig. 4(b) a close-up of this region for densities ranging from $\rho = 0.2$ to 0.8 is shown. To avoid a large scale in β_T the compressibility isochors are shifted by values given in Fig. 4(b). Using purely thermodynamic arguments Sastry *et al.*²⁵ showed that the isothermal compressibility β_T must increase upon isobaric cooling if the TMD line has a negative slope [$(\partial p / \partial T)_{\text{TMD}} < 0$] in the (p, T) plane. It is known that water shows an anomalous increase in β_T below $T = 46^\circ\text{C}$ corresponding to atmospheric pressure. Since the TMD line for the GCM has negative slope¹² it is of interest to investigate the β_T behavior at constant pressure. In Fig. 4(c), we show the temperature dependence of β_T for three different

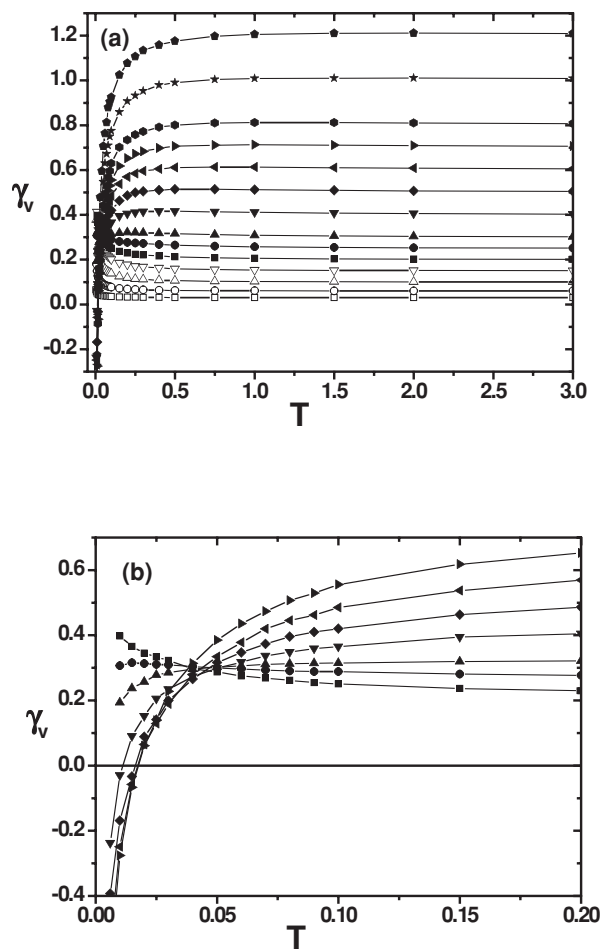


FIG. 3. Isothermal pressure coefficient γ_V as a function of temperature for different constant densities (a) ranging from $\rho = 0.03$ to 1.2 for temperatures up to $T = 3.0$ and (b) ranging from $\rho = 0.2$ to 0.7 for temperatures $T \leq 0.2$. Symbols are the same as in Fig. 1.

isobars between $p = 2.0$ and 3.0. Despite the fact that we computed this data directly from the numerical $p(\rho, T)$ values without any smoothing procedure β_T shows behavior similar to water with a clear minimum and the magnitude of β_T values are in good agreement with those given elsewhere.¹²

It is of interest to compare the isothermal and the adiabatic compressibility. In Fig. 5 the isothermal compressibility β_T (solid lines) and the adiabatic compressibility β_S (dashed lines) as a function of temperature at different constant densities is illustrated. In general, β_S lies below β_T except at the TMD where both compressibilities touch each other. The thermodynamic identities

$$C_P - C_V = \frac{T\beta_T\gamma_V^2}{\rho} \quad (8)$$

and

$$\frac{C_P}{C_V} = \frac{\beta_T}{\beta_S} \quad (9)$$

mean that C_P and C_V as well as β_T and β_S are equal at the TMD ($\gamma_V = 0$). A close-up of this region is shown in the inset of Fig. 5 where the curves are shifted by values given in parentheses.

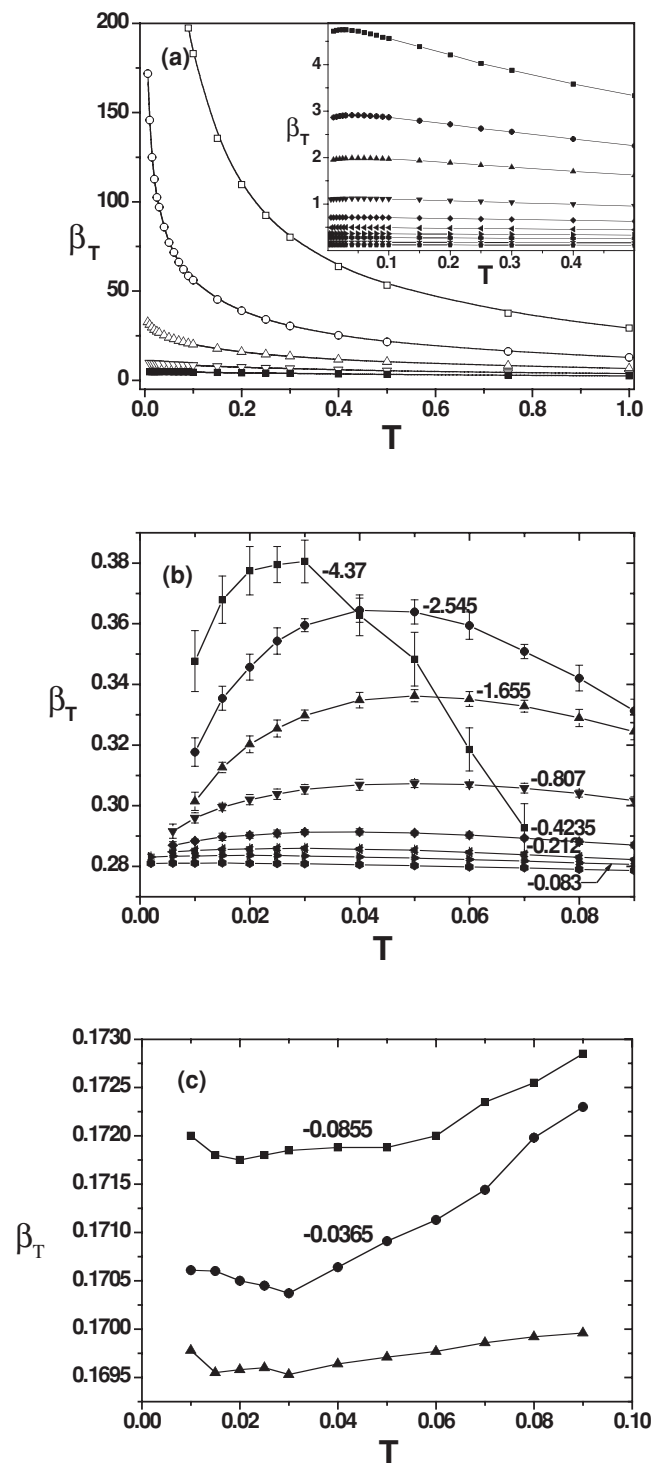


FIG. 4. (a) Isothermal compressibility β_T as a function of temperature for different constant densities ranging from $\rho = 0.03$ to 0.2 in the main frame and from $\rho = 0.2$ to 1.2 in the inset. (b) β_T -Isochores ranging from $\rho = 0.2$ to 0.8 for temperatures $T \leq 0.09$. Symbols are as in Fig. 1. (c) Isothermal compressibility β_T as a function of temperature for different constant pressures of $p = 2.0$ (■), 2.5 (●) and 3.0 (▲). The β_T -isochores in (b) and the isobars in (c) are shifted by values indicated on the lines in order to avoid a large scale.

D. Thermal expansion coefficient

For water, it is known that the thermal expansion coefficient α_p becomes negative below $T = 4^\circ\text{C}$ at atmospheric pressure. As a consequence of the thermodynamic identity

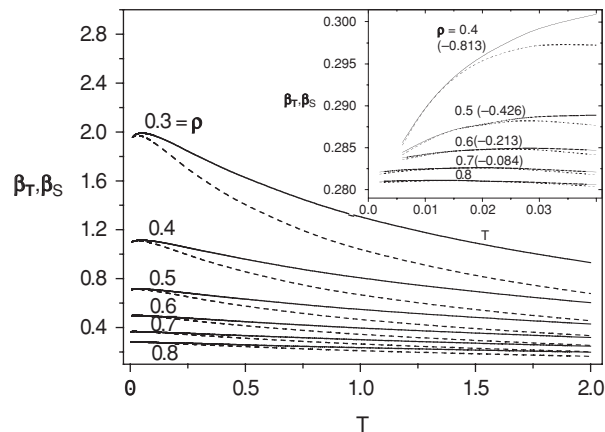


FIG. 5. Isothermal compressibility β_T (solid lines) and the adiabatic compressibility β_S (dashed lines) as a function of temperature for different constant densities ranging from $\rho = 0.3$ to 0.8 in the main frame and from $\rho = 0.4$ to 0.8 in the inset. In the inset the curves are shifted by values given in parentheses in order to avoid a large scale.

$\alpha_p = \gamma_V \beta_T$, this is also true for the GCM^{11,12} for state regions with $\gamma_V < 0$ since β_T is always positive in a one-phase region. In Fig. 6(a), we show the temperature dependence of α_p for different constant densities. Following the

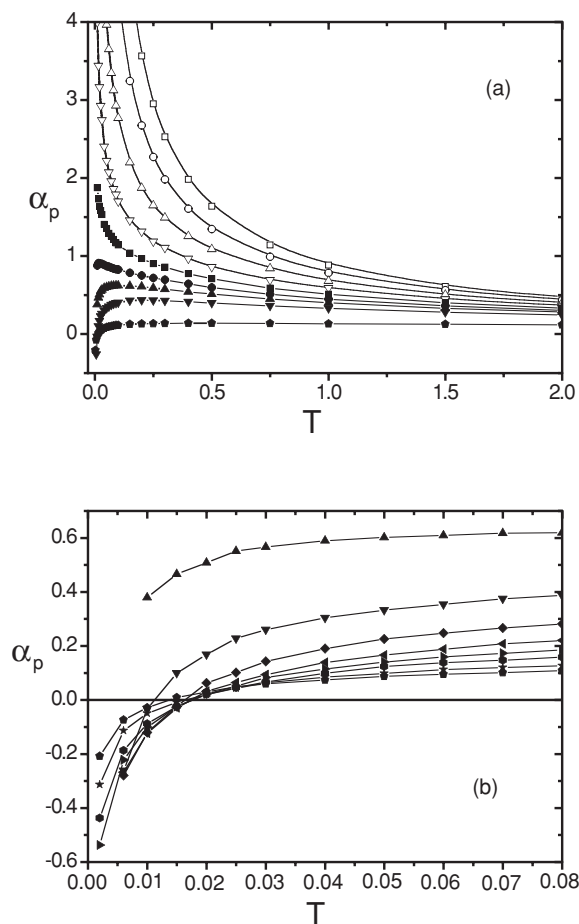


FIG. 6. The thermal expansion coefficient α_p as a function of temperature for different constant densities (a) ranging from $\rho = 0.03$ to 1.2 for temperatures up to $T = 2.0$ and (b) ranging from $\rho = 0.3$ to 1.2 for temperatures $T \leq 0.08$. Symbols are as in Fig. 1.

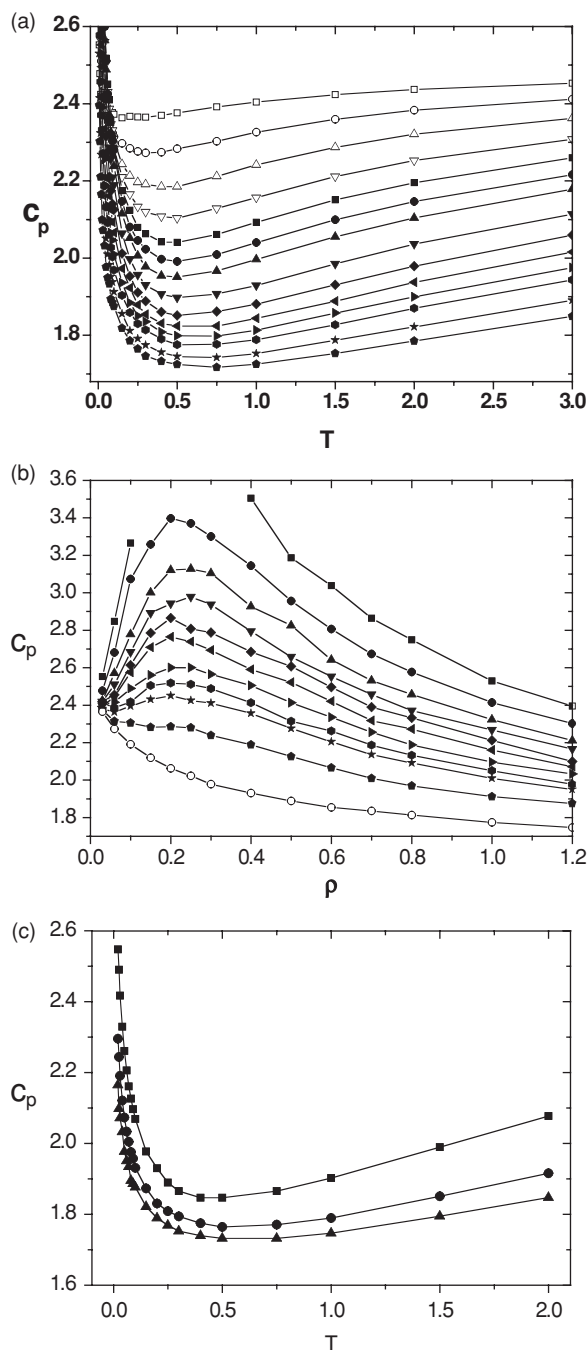


FIG. 7. (a) Specific heat C_p at constant pressure as a function of temperature for different constant densities ranging from $\rho = 0.03$ to 1.2. Symbols are as in Fig. 1. (b) C_p as a function of density for different constant temperatures of $T = 0.006$ (■), 0.01 (●), 0.015 (▲), 0.02 (▼), 0.025 (◆), 0.03 (◄), 0.04 (►), 0.05 (●), 0.06 (★), 0.1 (●), 0.3 (○). (c) C_p as a function of temperature for different constant pressures of $p = 1.0$ (■), 2.5 (●) and 4.0 (▲).

behavior of β_T at low densities the thermal expansion coefficient α_p decreases sharply with increasing temperature for densities ranging from $\rho = 0.03$ to 0.2 [see Fig. 6(a)]. In the range of $\rho = 0.25$ to 0.4 α_p exhibits a maximum at low temperature. Negative thermal expansion coefficients occur for $\rho \geq 0.4$ and low temperature. In Fig. 6(b), a close-up of this region for densities ranging from $\rho = 0.3$ to 1.2 is shown.

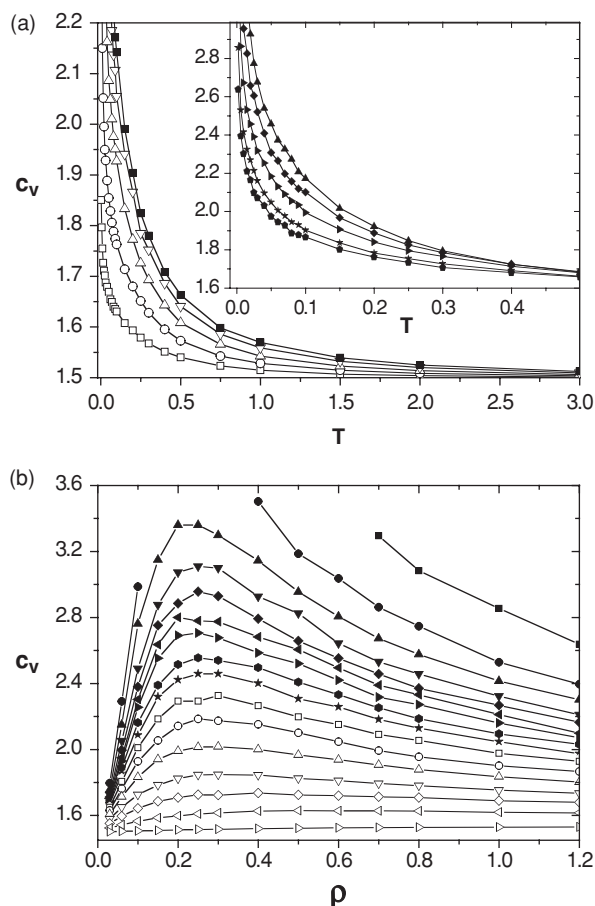


FIG. 8. (a) Specific heat C_v at constant volume as a function of temperature for different constant densities ranging from $\rho = 0.03$ to 1.2 in the main frame and from $\rho = 0.3$ to 1.2 in the inset. Symbols are as in Fig. 1. (b) C_v as a function of density for different constant temperatures of $T = 0.006$ (■), 0.006 (●), 0.01 (▲), 0.015 (▼), 0.02 (◆), 0.025 (◄), 0.03 (►), 0.04 (●), 0.05 (★), 0.07 (□), 0.1 (○), 0.15 (△), 0.25 (▽), 0.4 (◇), 0.75 (◁), 3.0 (▷).

E. Isobaric and isochoric heat capacities

In Fig. 7(a), the temperature dependence of the constant pressure heat capacity C_p is shown along various isochors ranging from $\rho = 0.03$ to 1.2. C_p rises sharply in the vicinity of the solid–liquid phase boundary. When the temperature is increased, C_p passes through a minimum, followed by a further increase upon further heating. The density dependence of C_p for different constant temperatures ranging from $T = 0.006$ to 0.3 is shown in Fig. 7(b). The heat capacity isotherms show a pronounced maximum at about $\rho \approx 0.25$ that disappears at a temperature of approximately $T \approx 0.09$.

In normal liquids, the heat capacity increases with increasing temperature at constant pressure. Contrary to this behavior the heat capacity of water has a minimum at $T = 36^\circ\text{C}$ at atmospheric pressure. Against this background, it is of interest to see whether or not the minimum in C_p along isochors [Fig. 7(a)] also exists at constant pressure. In Fig. 7(c), we show the temperature dependence of C_p for three different isobars between $p = 1.0$ and 4.0. Similar to water the GCM heat capacity C_p shows a clear anomalous minimum along isobars.

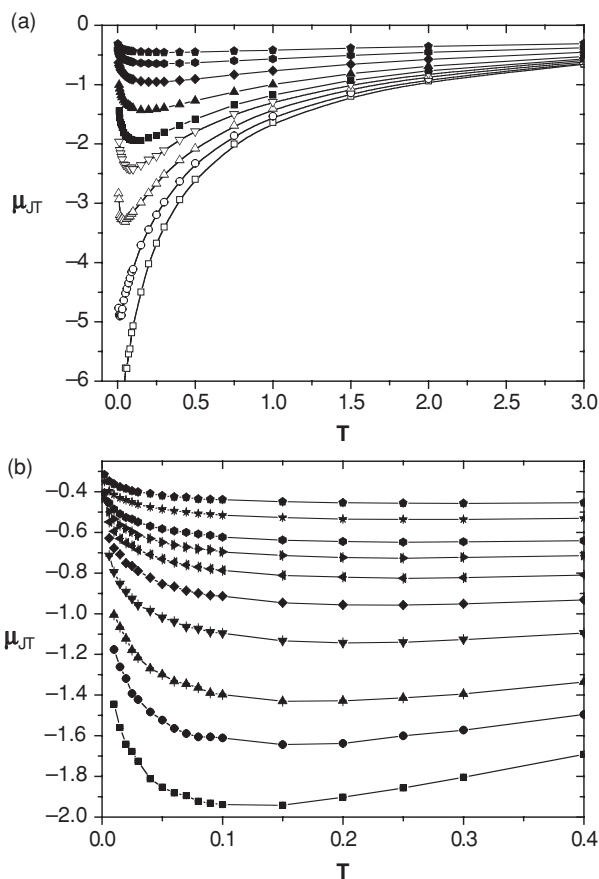


FIG. 9. Joule–Thomson coefficient μ_{JT} as a function of temperature for different constant densities (a) ranging from $\rho = 0.03$ to 1.2 for temperatures up to $T = 3.0$ and (b) ranging from $\rho = 0.2$ to 1.2 for temperatures $T \leq 0.4$. Symbols are the same as in Fig. 1.

The constant volume heat capacity C_V as a function of temperature at different constant densities is illustrated in Fig. 8(a). Similar to the C_P behavior the specific heat at constant volume C_V increases sharply near the solid–liquid transition line. Contrary to the C_P behavior C_V decreases monotonically with increasing temperature without a minimum. For densities ranging from $\rho = 0.03$ to 0.2 C_V increases at constant temperature and for densities from $\rho = 0.3$ to 1.2 [shown in the inset of Fig. 8(a)] C_V decreases at constant temperature indicating a maximum in C_V along isotherms as discussed in connection with equation (7). This can be seen clearly in Fig. 8(b) where the density dependence of C_V for different constant temperatures ranging from $T = 0.002$ to 3.0 is illustrated. As discussed above a pronounced maximum in C_V occurs at low temperatures at a density of approximately $\rho = 0.25$. The maximum disappears at higher temperatures.

F. Joule–Thomson coefficient

In Fig. 9(a), the isochoric temperature dependence of the Joule–Thomson coefficient μ_{JT} is shown. At a density of $\rho = 0.03$ μ_{JT} grows monotonically with increasing temperature showing a strong gradient at low temperatures. For densities $\rho \geq 0.06$, the slope of μ_{JT} exhibits a minimum at low temperatures with strong negative gradients near the liquid–solid transition. Figure 9(b) shows a close-up of this region for densities

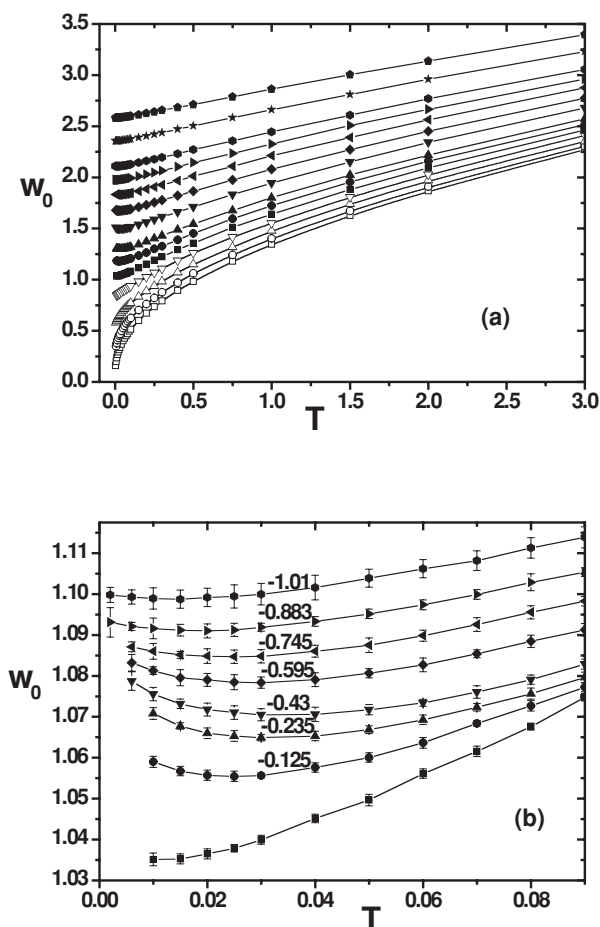


FIG. 10. Zero frequency speed of sound w_0 as a function of temperature for different constant densities (a) ranging from $\rho = 0.03$ to 1.2 for temperatures up to $T = 3.0$ and (b) ranging from $\rho = 0.2$ to 0.8 for temperatures $T \leq 0.09$. In (b) the speed of sound isochors are shifted by values indicated on the lines in order to avoid a large scale in w_0 . Symbols are the same as in Fig. 1.

ranging from $\rho = 0.2$ to 1.2. The minimum in μ_{JT} is shifted to higher temperatures when the density increases. In general, the Joule–Thomson coefficient is negative in the whole range we have simulated. Therefore, the GCM system does not exhibit a Joule–Thomson inversion curve defined by $\mu_{JT} = 0$.

G. Speed of sound

The zero frequency speed of sound w_0 as a function of temperature at different constant densities is illustrated in Fig. 10(a). For densities ranging from $\rho = 0.03$ to 0.15, the speed of sound increases with increasing temperature similar to normal liquids. Contrary to simple liquid behavior, w_0 develops a clear anomalous minimum along isochors for densities $\rho \geq 0.2$ at low temperatures. Figure 10(b) shows a close-up of this region for densities ranging from $\rho = 0.2$ to 0.8, where the w_0 isochors are shifted by values given in the figure in order to avoid a large w_0 scale. It is known that water exhibits an anomalous maximum in the speed of sound at $T = 74^\circ\text{C}$ at atmospheric pressure.²⁶ The maximum is shifted to higher temperatures when the pressure increases. Within the accuracy of our simulation data we could not find a maximum in the speed of sound along isobars for the GCM system.

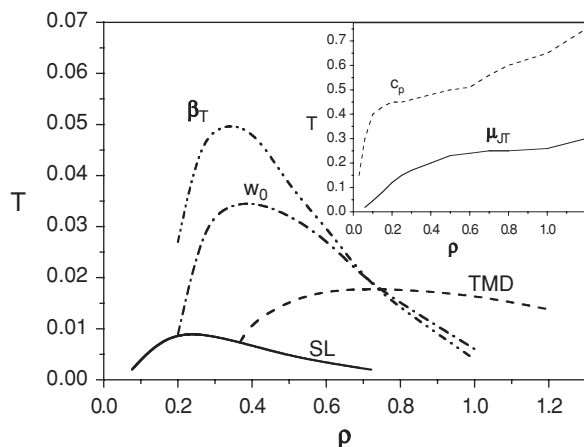


FIG. 11. Course of thermodynamic state variable—extrema along isochors in the ρ, T —projection. Main frame: TMD line (dashed line), minima in w_0 (dashed dotted line), maxima in β_T (dashed dot dotted line) and solid–liquid coexisting line (Ref. 17) (solid line). In the inset: Minima of C_p (dashed line) and minima of μ_{JT} (solid line).

H. Comparison of the extrema of thermodynamic state variables

The course of all extrema found for the thermodynamic state values along isochors in the ρ, T projection is shown in Fig. 11. In addition to the solid–liquid coexisting line¹⁷ and the TMD line we show the course of the minima in w_0 as well as the maxima in β_T along isochors. Both extrema lines approximately cross each other at the maximum of the TMD line. For densities lower than the crossing point the β_T extrema line encloses the w_0 extrema line. In the inset of Fig. 11 we show the course of the minima of C_p and μ_{JT} along isochors. Both extrema are shifted to higher temperatures when the density increases. In general, the C_p minima occur at higher temperatures than the μ_{JT} minima.

IV. CONCLUSIONS

Extensive MD simulations for an NVEPG ensemble were conducted to obtain the general thermodynamic behavior for the GCM fluid for a wide range of both density and temperature. We applied a method where, in principle, all thermodynamic state variables can be determined directly from MD simulations. In this approach, the thermodynamic state variables are expressible in terms of phase-space functions which involve ensemble averages of products of powers of the kinetic energy and of volume derivatives of the potential energy.

In addition to the waterlike anomalies such as density maximum, negative thermal expansion coefficient,¹¹ and anomaly in the isothermal compressibility¹² we also found additional peculiarities in the GCM for the isothermal pressure coefficient, the constant pressure heat capacity, the zero frequency speed of sound and the Joule–Thomson coefficient.

To the best of our knowledge, this is the first application of the NVEPG ensemble to derive thermodynamic properties of a fluid system for such an extensive range of both temperature and density. We believe that the systematic approach used here can also contribute to the improved understanding of the thermodynamic properties of fluids in general.

ACKNOWLEDGMENTS

Financial support from the Deutsche Forschungsgemeinschaft (DFG) is gratefully acknowledged.

- ¹R. Lustig, *J. Chem. Phys.* **100**, 3048 (1994).
- ²R. Lustig, *J. Chem. Phys.* **100**, 3060 (1994).
- ³R. Lustig, *J. Chem. Phys.* **100**, 3068 (1994).
- ⁴R. Lustig, *J. Chem. Phys.* **109**, 8816 (1998).
- ⁵K. Meier and S. Kabelac, *J. Chem. Phys.* **124**, 064104 (2006).
- ⁶E. M. Pearson, T. Halicioglu, and W. A. Tiller, *Phys. Rev. A* **32**, 3030 (1985).
- ⁷T. Çağın and J. R. Ray, *Phys. Rev. A* **37**, 247 (1988).
- ⁸T. Çağın and J. R. Ray, *Phys. Rev. A* **37**, 4510 (1988).
- ⁹F. H. Stillinger, *J. Chem. Phys.* **65**, 3968 (1976).
- ¹⁰C. N. Likos, *Phys. Rep.* **348**, 267 (2001).
- ¹¹F. H. Stillinger and D. K. Stillinger, *Physica A* **244**, 358 (1997).
- ¹²P. Mausbach and H.-O. May, *Fluid Phase Equilib.* **249**, 17 (2006).
- ¹³W. P. Krekelberg, T. Kumar, J. Mittal, J. R. Errington, and T. M. Truskett, *Phys. Rev. E* **79**, 031203 (2009).
- ¹⁴A. Lang, C. N. Likos, M. Watzlawek, and H. Löwen, *J. Phys.: Condens. Matter* **12**, 5087 (2000).
- ¹⁵P. V. Giaquinta and F. Saija, *ChemPhysChem* **6**, 1768 (2005).
- ¹⁶S. Prestipino, F. Saija, and P. V. Giaquinta, *Phys. Rev. E* **71**, 050102(R) (2005).
- ¹⁷P. Mausbach, A. Ahmed, and R. J. Sadus, *J. Chem. Phys.* **131**, 184507 (2009).
- ¹⁸P. Mausbach and H.-O. May, *Proc. Appl. Math. Mech.* **5**, 685 (2005).
- ¹⁹H.-O. May and P. Mausbach, *Phys. Rev. E* **76**, 031201 (2007).
- ²⁰P. Mausbach and H.-O. May, *Z. Phys. Chem.* **223**, 1035 (2009).
- ²¹P. Mausbach and H.-O. May, *Proc. Appl. Math. Mech.* **8**, 10631 (2008).
- ²²A. Ahmed, P. Mausbach, and R. J. Sadus, *J. Chem. Phys.* **131**, 224511 (2009).
- ²³A. Ahmed, P. Mausbach, and R. J. Sadus, *Phys. Rev. E* **82**, 011201 (2010).
- ²⁴C. W. Gear, *Numerical Initial Value Problems in Ordinary Differential Equations* (Prentice-Hall, Englewood Cliffs, NJ, 1971).
- ²⁵S. Sastry, P. G. Debenedetti, F. Sciortino, and H. E. Stanley, *Phys. Rev. E* **53**, 6144 (1996).
- ²⁶G. Benedetto, R. M. Gaviolo, P. A. Giuliano Albo, S. Lago, D. Madonna Ripa, and R. Spagnolo, *Int. J. Thermophys.* **26**, 1667 (2005).